Probabilistic Multi-hazard Shaking-Tsunami Risk Assessment for the District of Tofino, British Columbia, Canada, Subjected to Megathrust Cascadia Subduction Events

Katsuichiro Goda
Associate Professor, Dept. of Earth Sciences, Western University, London, Ontario, Canada

ABSTRACT: A probabilistic earthquake-tsunami risk model is developed to quantify the financial impacts of the future megathrust events from the Cascadia subduction zone (CSZ) to coastal communities in the Pacific Northwest. The model is developed by focusing on the District of Tofino, British Columbia (BC), where high-quality building exposure data and high-resolution bathymetry-elevation data are available. To account for uncertainties associated with earthquake ruptures, stochastic source modeling is adopted. The multi-hazard risk assessment is carried out by identifying critical earthquake scenarios that correspond to different return periods. Results indicate that ground shaking is the primary contributor of the total risk but at longer return period levels, the contribution from tsunami becomes significant, highlighting the importance of multi-hazard risk assessments for improved disaster risk management.

1. INTRODUCTION

Southwestern BC has a high likelihood of facing significant earthquakes in the future and is exposed to major seismic and tsunami hazards, originating from the CSZ (Satake et al., 2003; Goldfinger et al., 2012). The Cascadia region involves the thrusting movements of the Juan de Fuca, Gorda, and Explorer Plates, which subduct underneath the North American Plate. A scenario of particular concern to residents and emergency managers is the future occurrence of a moment magnitude (M) 9.0-class megathrust earthquake in Cascadia (Leonard et al., 2014). The scientific challenges in assessing the potential georisks include the characterization of the earthquake rupture of future major Cascadia events and the modeling of their multi-hazard cascades which affect the population and built environment simultaneously. Coastal communities on Vancouver Island face urgent needs for operational decision-support tools that provide accurate performance assessments of buildings and infrastructures under multi-hazard actions.

This study presents a probabilistic earthquake-tsunami risk model for the CSZ using the latest information on earthquake occurrence, rupture pattern, fault plane, and source characteristics. The earthquake occurrence and rupture models for the CSZ are developed by incorporating the time-dependency of earthquake occurrence (Goda, 2019) and by adopting a stochastic rupture modeling approach to consider heterogeneous slip distributions (Goda, 2022). Subsequently, a probabilistic earthquake-tsunami risk analysis is performed by focusing on the District of Tofino, BC, which is exposed to the Cascadia megathrust earthquakes. Results produce multi-hazard loss estimations for shaking and tsunami and help identify critical scenarios at different return period levels that are relevant for earthquake risk management, highlighting the relative impacts of shaking and tsunami risks. The results are beneficial for creating joint maps of shaking and tsunami risks for coastal communities in Canada and for promoting multi-hazard risk mitigation actions against the future Cascadia events.

2. MULTI-HAZARD RISK MODEL FOR TOFINO UNDER CASCADIA EVENTS

This section presents a multi-hazard shaking-tsunami risk model for Tofino due to the Cascadia subduction earthquakes. An overall methodology is illustrated in Figure 1, consisting of an earthquake occurrence model, stochastic rupture model, shaking hazard-risk model, tsunami

hazard-risk model, and multi-hazard loss estimation. Key features of the above-mentioned model components are described below. The approach is similar to Goda and De Risi (2018).

2.1. Cascadia subduction zone and building exposure data for Tofino

The earthquake rupture characterization of the Cascadia events has evolved over the last three decades (Walton et al., 2021). A map of the CSZ is shown in Figure 2a. Early models of the subduction zone geometry were constrained by geodetic deformation data, thermal models, seismic reflection/refraction data, and deep seismicity data. The Slab2 model includes the latest fault interface geometry for the CSZ (Hayes et al., 2018). To predict the future rupture patterns of the CSZ events, geological and geophysical evidence and data have been collected, including onshore subsidence records and offshore marine turbidites (Goldfinger et al., 2012).

Tofino is located at the tip of Esowista Peninsula on Vancouver Island and is exposed to the Pacific to its west. A map of Tofino, including buildings and roads, is shown in Figure 2b. For shaking-tsunami risk assessments, a portfolio of 1,789 buildings is considered. Most buildings are 1- to 2-story wooden houses and were constructed in 1960s or afterwards. The total value of a building is typically less than C$ 2 million with the average value of C$ 1.27 million. The total asset value of the 1,789 buildings is C$ 2.27 billion. The average footprint area of the 1,789 buildings is 181.8 m^2. The cost information of the

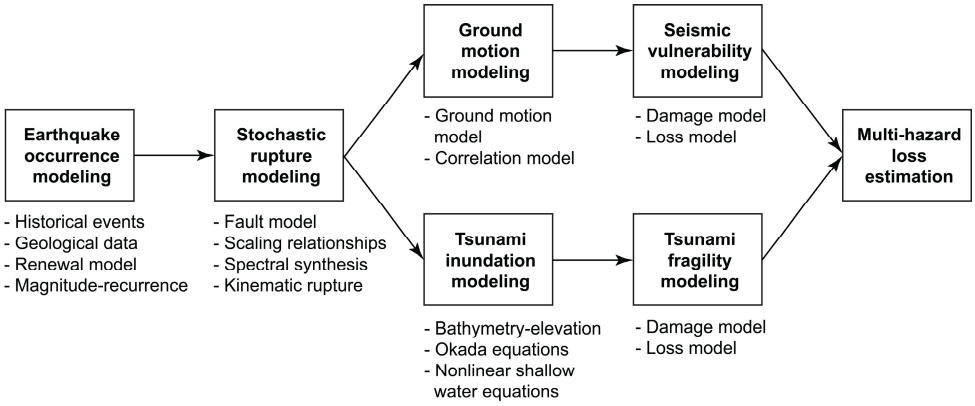

Figure 1: Flowchart of multi-hazard shaking and tsunami loss estimation.

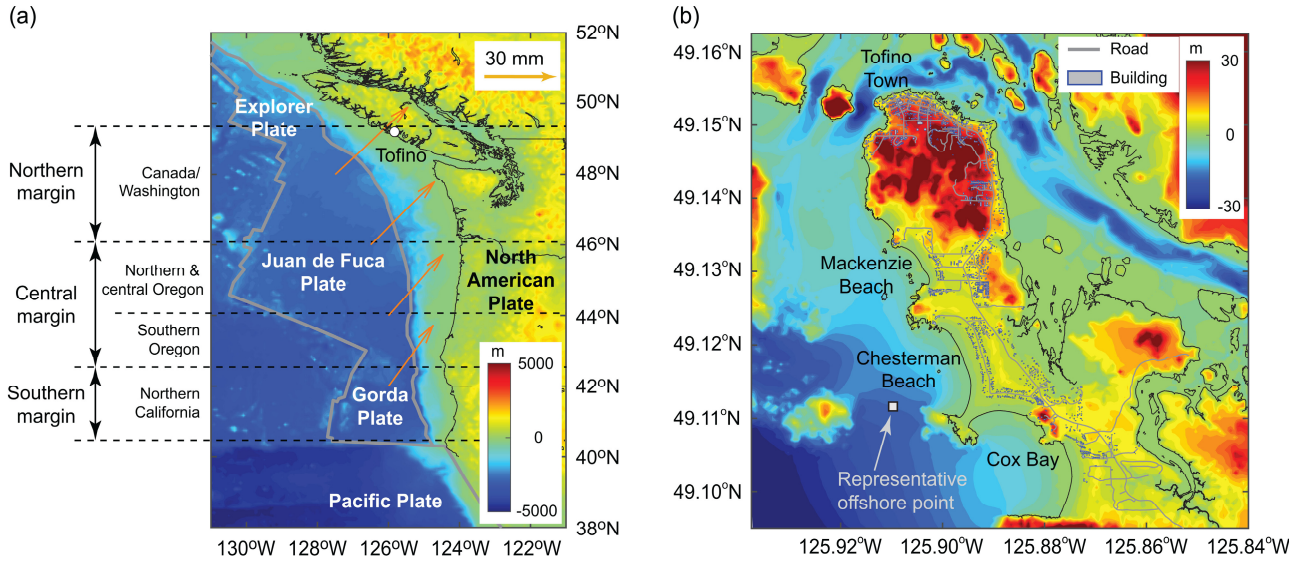

Figure 2: (a) Tectonic plates surrounding the CSZ. (b) Map of Tofino (bathymetry-elevation, buildings, and roads).

individual buildings is used in the shaking-tsunami loss estimation. From tsunami hazard viewpoints, many buildings in Tofino Town are at relatively high elevations and are protected from direct tsunami waves. In contrast, buildings in beach areas are at low elevations and face the Pacific Ocean directly. Consequently, the latter areas are exposed to significant tsunami hazards.

2.2. Earthquake occurrence model

Earthquake occurrence from the CSZ is non-Poissonian (Goldfinger et al., 2012). A renewal process is suitable for such a non-Poisson process, where interarrival time distribution of earthquakes is used to characterize the evolution of occurrence probability with time. The earthquake data obtained from 40 events over the last 10,000 years, identified by Goldfinger et al. (2012), can be used to determine a suitable interarrival time distribution and parameters (i.e., mean recurrence and coefficient of variation).

The historical rupture patterns of the CSZ show whole and segmented ruptures with different fault lengths. To account for different rupture patterns, two earthquake occurrence models are developed. One is to use all 40 identified earthquakes in determining the occurrence of different segmented ruptures in the Cascadia region. In this case, earthquake scenarios having M8.1 to M9.1 are considered comprehensively. An alternative approach is to focus on the full-margin rupture only and to characterize its rupture using 19 whole rupture events. In this case, the corresponding earthquake magnitudes are between M8.7 to M9.1. The focus on the whole rupture scenarios is justified, because tsunamis caused by central and southern margins of the CSZ are unlikely to generate significant tsunamis along the Canadian coast due to their tsunami radiation patterns (Goda, 2022).

To identify the suitable interarrival time distributions for the CSZ data, exploratory analyses are performed by considering several probability distributions (e.g., normal, exponential, lognormal, and Weibull). The model selection based on the Akaike Information Criterion indicates that the Weibull distribution is suitable for characterizing the interarrival time data from the CSZ. When the segmented rupture scenarios are considered, the mean recurrence period and the coefficient of variation are estimated to be 244 years and 0.50, respectively. When the whole rupture scenarios are considered, the mean recurrence period and the coefficient of variation are estimated to be 529 years and 0.51, respectively. The elapsed time since the 1700 CSZ event is 322 years, and this information is incorporated in modeling the time-dependent earthquake occurrence from the CSZ.

The earthquake magnitude distribution is critical for seismic and tsunami hazard assessments. The magnitudes of the CSZ are primarily dependent on the rupture patterns (i.e., segmented versus whole ruptures). In this study, the magnitude distribution is characterized by the Gutenberg-Richter model with the b-value of 1. The minimum and maximum magnitudes are set to 8.1 and 9.1 for the segmented rupture scenarios and to 8.7 and 9.1 for the whole rupture scenarios.

2.3. Stochastic rupture model

The fault plane geometry for the CSZ is based on the Slab2 model (Hayes et al., 2018). This fault plane is approximated by a set of 7,452 sub-faults that reach depths of 30 km. Each sub-fault has the size of 5.6 km along the strike and 3.8 km along the dip. To synthesize the earthquake slip distribution, a scenario magnitude is specified with a 0.1 magnitude bin and the magnitude value is simulated from the uniform distribution. Subsequently, eight earthquake source parameters, i.e., fault length, fault width, mean slip, maximum slip, Box-Cox parameter, along-strike correlation length, along-dip correlation length, and Hurst number, are sampled from the statistical scaling relationships by Goda et al. (2016). These parameters are represented by the multi-variate lognormal distribution. Once a suitable fault geometry is determined, the fault plane is placed randomly within the CSZ.

For a given fault plane geometry, a heterogeneous earthquake slip distribution is synthesized. A candidate slip distribution is first simulated from an anisotropic von Kármán

wavenumber spectrum with its amplitude spectrum being parametrized by along-strike correlation length, along-dip correlation length, and Hurst number and its phase being randomly distributed between 0 and 2π (Mai and Beroza, 2002). The simulated slip distribution is modified via Box-Cox power transformation to achieve a desirable right-skewed feature of the marginal slip distribution (Goda et al., 2016). To ensure that the simulated earthquake slip distribution has realistic characteristics for the target CSZ events, several constraints on the simulated slip distribution are implemented. For instance, major asperities are constrained to occur in the shallow part of the subduction interface to broadly coincide with the outer wedge of the accretionary prism. If the candidate slip distribution does not meet all criteria, this realization is discarded, and another stochastic rupture model is generated. This process is iterated until an acceptable model is obtained. By repeating the above procedure 500 times for each of the ten bins between *M*8.1 and *M*9.1, a set of 5,000 earthquake rupture models is generated (Goda, 2022). The stochastic rupture models can represent different fault geometry, positions within the overall fault plane of the CSZ, and heterogenous earthquake slip distributions.

2.4. Ground shaking hazard-risk model

To generate seismic intensities at building sites in Tofino, ground motion models for the Cascadia subduction events by Atkinson and Adams (2013) are used. The ground motion models include three logic-tree branches (best/lower/upper) with weights of 0.5, 0.2, and 0.3, respectively. The same ground motion models were used in the 5th generation national seismic hazard maps in Canada. The seismic intensity measures are spectral accelerations at 0.3 s (1763 buildings) and 0.5 s (26 buildings) based on seismic vulnerability functions for the buildings in Tofino (see the next paragraph). The local site information is represented by average shear wave velocities in the uppermost 30 m, determined based on horizontal-to-vertical spectral ratio measurements. To adjust for site responses, the site amplification factors that were implemented in the 2015 National Building Code of Canada are applied. Moreover, to account for realistic spatial variations of spectral accelerations at different sites and periods, an intra-event spatial correlation model by Goda and Atkinson (2010) is implemented by simulating correlated normally distributed error terms.

Seismic vulnerability models quantify the degree of seismic loss to a building as a function of seismic intensity. The seismic vulnerability functions for buildings in Tofino are obtained from the Open Disaster Risk Reduction program (https://opendrr.github.io/downloads/en/), created by the Geological Survey of Canada. The seismic vulnerability functions are defined by a mean loss ratio as a function of spectral acceleration at a vibration period. For each structure, a building system and total asset value are represented by structural, non-structural, and contents elements, and for each building element, an applicable mean seismic vulnerability function is specified. Figure 3 shows mean seismic vulnerability functions of structural, non-structural, and contents elements, respectively, for a residential building class RES1-W1-LC, which is most prevalent in Tofino. To account for uncertainty associated with seismic damage assessment and loss estimation, a lognormal random variable with the mean loss predicted by the vulnerability functions and the coefficient of variation equal to 0.3 is used for simulating the loss ratios.

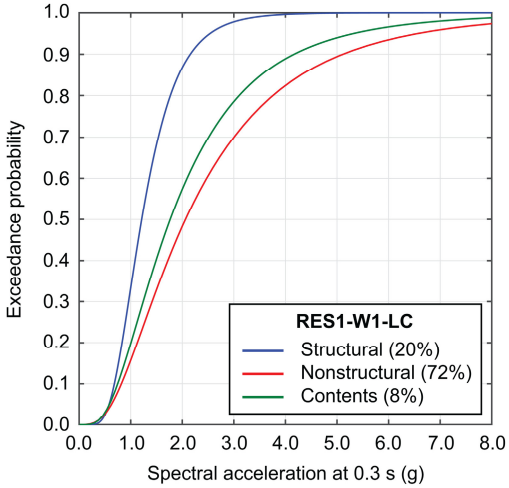

Figure 3: Shaking vulnerability functions for a residential wooden building.

2.5. Tsunami hazard-risk model

To evaluate tsunami inundations in Tofino by considering numerous stochastic earthquake rupture models (Section 2.3), ground deformations due to earthquake ruptures are calculated using Okada (1985) equations and then nonlinear shallow water equations are solved using the TUNAMI code (Goto et al., 1997). For this purpose, nested grids of 810-m, 270-m, 90-m, 30-m, 10-m, and 5-m that cover the entire CSZ are set up by combining global bathymetry data (GEBCO–450-m), national bathymetry data (CHS–10-m) and elevation data (CDEM–20-m), and LiDAR-derived topographic contours (0.5-m). The high-resolution local elevation data cover the District of Tofino (Figure 2b). The vertical reference datum is at the mean sea level. For all computational cells, the bottom friction and surface roughness are represented by a Manning's coefficient equal to 0.025 $m^{-1/3}s$, which is often used for agricultural land and ocean/water. The run-up calculation is determined by evaluating a dry/wet condition of a computational cell based on total water depth relative to its elevation. Moreover, the effects of coseismic ground deformation are considered by adjusting the elevation data prior to the tsunami simulation run.

Each tsunami simulation is performed for a 3-hour duration which is sufficient to model the most critical phase of tsunami waves for the Cascadia tsunami scenarios. To perform numerous inundation analyses efficiently, tsunami simulations for offshore sites are run by considering the 270-m grids and all 5,000 earthquake rupture models between *M*8.1 and *M*9.1. In addition, high-resolution inundation simulations are run using 5-m grids by focusing on 1,000 stochastic rupture models of the Cascadia full-margin scenarios (*M*8.7 to *M*9.1).

In quantifying tsunami risks for buildings in Tofino, an empirical tsunami fragility model by De Risi et al. (2017) is adopted, which was developed based on the tsunami damage data from the 2011 Tohoku event in Japan, containing more than 200,000 observations. The tsunami fragility model is characterized using multinomial logistic regression analysis by considering the structural typology (i.e., wood, concrete, steel, and masonry and others), number of stories, and topographical indicators (i.e., coastal plain and ria) as explanatory variables.

Figure 4 shows tsunami fragility functions of wooden buildings for five tsunami damage levels, i.e., minor, moderate, extensive, complete, and collapse. For tsunami loss estimation, these tsunami damage levels are related to building damage ratio ranges of 0.03–0.1, 0.1–0.3, 0.3–0.5, 0.5–1.0, and 1.0, respectively (http://www.mlit.go.jp/toshi/toshi-hukkou-arkaibu.html). During the tsunami damage and loss analyses, the tsunami fragility functions are applied using inundation depth values at individual buildings. The damage states are assigned probabilistically by comparing a uniform random number between 0 and 1 with the corresponding tsunami damage probabilities. If the random number falls within the range of tsunami damage probabilities for a specific damage level, the tsunami damage state is selected, and subsequently, the tsunami damage ratio is sampled within the suggested range. Finally, the tsunami loss value is determined by multiplying the total asset value of the property and the sampled damage ratio. The above procedure is repeated for all buildings for a given inundation scenario.

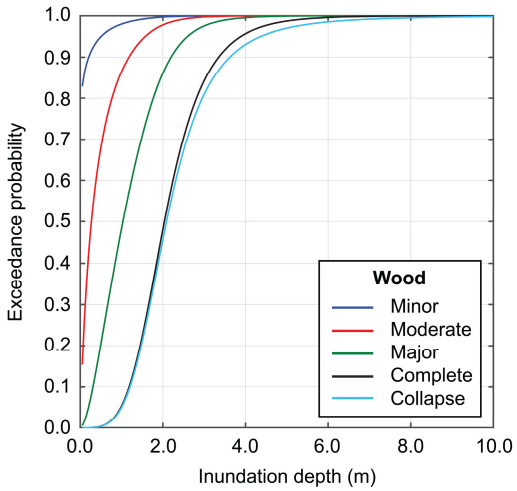

Figure 4: Tsunami fragility functions of wooden buildings based on De Risi et al. (2017).

3. MULTI-HARZAD LOSS ESTIMATION FOR BUILDINGS IN TOFINO

In this study, the multi-hazard loss estimation for ground shaking and tsunami due to the CSZ events is conducted in two steps. Section 3.1 describes an approach to select critical earthquake scenarios based on probabilistic tsunami hazard analysis. Section 3.2 presents multi-hazard loss estimation results based on probabilistic shake map generation and high-resolution tsunami inundation simulations.

3.1. Critical earthquake rupture scenarios based on probabilistic tsunami hazard analysis

In the first step, time-dependent probabilistic tsunami hazard analysis is carried out by considering two earthquake occurrence models (i.e., segmented and whole rupture cases; Section 2.2) and by considering 5,000 stochastic rupture scenarios (Section 2.3). The tsunami simulations are based on 270-m grid resolutions (Section 2.5). The numerical procedure of the time-dependent probabilistic tsunami hazard analysis is the same as Goda (2019). Figure 5 shows a tsunami hazard curve for a representative offshore location near Tofino (see Figure 2b). In the curve, five representative return period levels (i.e., 200, 500, 1000, 2500, and 5000 years) are indicated. For each return period level, multiple critical earthquake rupture models can be assigned. For instance, the return period of 200 years can be represented by a *M*8.5 scenario that ruptures the central segment of the CSZ off Oregon and causes a small-amplitude tsunami wave of 0.46 m. On the other hand, when the return period is increased to 2500 years, a *M*9.0 whole rupture scenario becomes dominant and causes a significant tsunami wave of 6.93 m. With the increase of the return period, critical earthquake rupture models tend to have significant earthquake slip asperities in the near-trench region, spanning across the whole margin. The tsunami hazard analysis facilitates the identification of critical rupture scenarios that lead to significant tsunami hazards.

For Tofino, all major tsunami scenarios above the return period of 500 years come from the whole rupture scenarios having the earthquake magnitudes between *M*8.7 and *M*9.1 and site-to-rupture distances of 20 km (this approximately corresponds to the closest 3D distance from Tofino to the CSZ fault plane). From seismic hazard viewpoints, the expected ground shaking for buildings in Tofino is similar regardless of different critical rupture scenarios that are identified through probabilistic tsunami hazard analysis (Figure 5). This insensitivity of the ground shaking hazard (and risk) to different critical rupture scenarios is attributed to the parametrization of the current generation of ground motion models for the megathrust interface events, whose predictions of ground shaking only depend on the earthquake magnitude and the source-to-site distance.

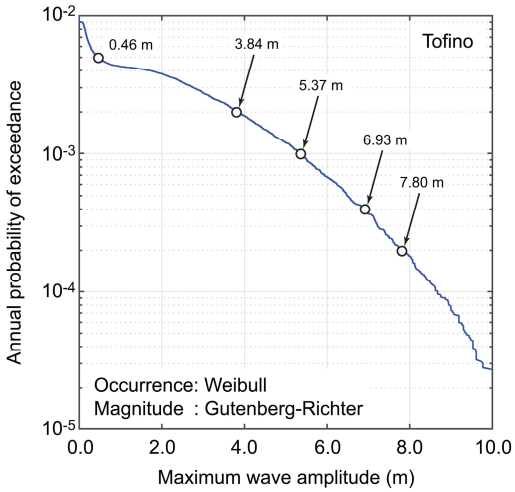

Figure 5: Tsunami hazard curve for the representative offshore location near Tofino.

3.2. Multi-hazard loss estimation for Tofino

In the second step, probabilistic shake maps are generated, and high-resolution tsunami simulations are performed for the critical scenarios that are identified in Section 3.1. Shaking and tsunami risks can be evaluated for individual buildings and portfolio-level shaking and tsunami risks can be assessed by aggregating the individual losses. In this study, the multi-hazard building loss is evaluated by taking the larger estimated loss from shaking and tsunami. This approach is simplistic and ignores the damage accumulation in a building due to a sequential shaking-tsunami load.

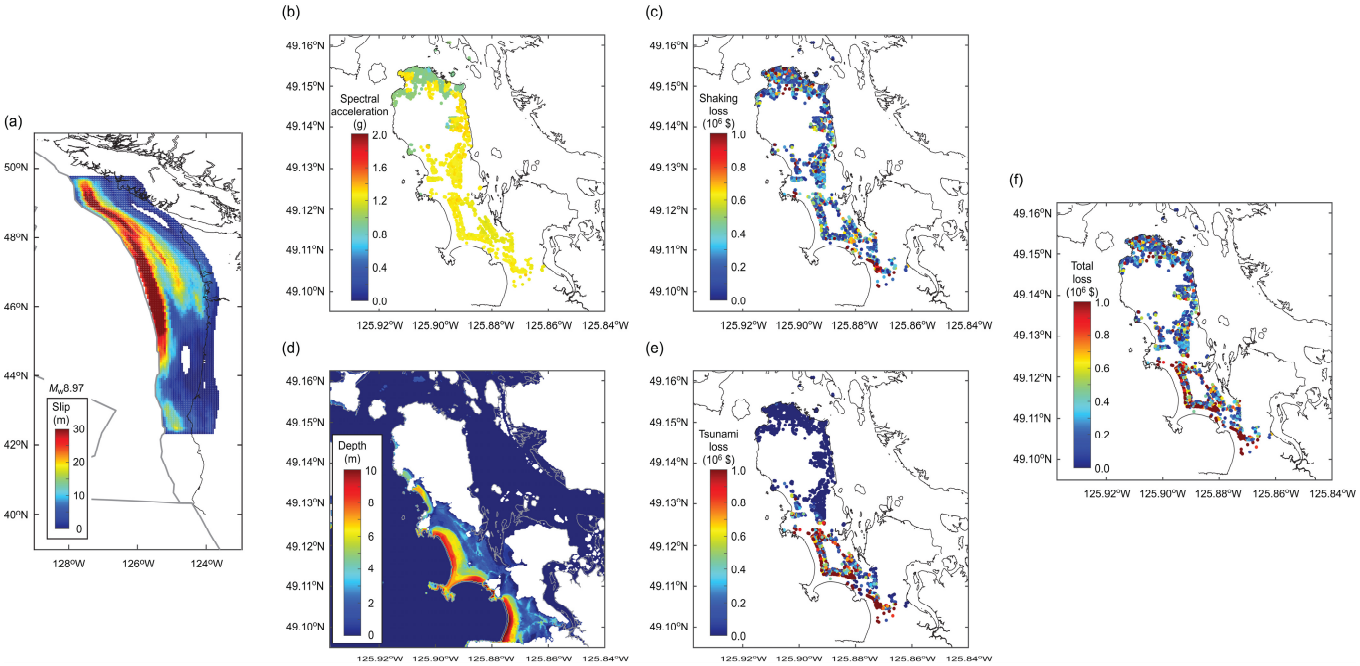

Figure 6: An example of shaking-tsunami loss estimation for Tofino by considering the M8.97 full-rupture earthquake scenario at the 2500-year return period level: (a) earthquake slip distribution, (b) shake map, (c) shaking loss distribution, (d) inundation depth, (e) tsunami loss distribution, and (f) combined shaking-tsunami loss distribution.

To illustrate the multi-hazard loss estimation procedure, Figure 6 presents the shaking-tsunami loss estimation results for the return period of 2500 years. Figure 6a shows the earthquake slip distribution of the critical rupture scenario.

For the shaking hazard and risk assessments, the average ground shaking values at the building sites for the critical scenario is presented in Figure 6b. The expected shaking level exceeds 1.0 g (note: the majority of the buildings are based on the spectral acceleration at 0.3 s). The sites with yellow colors have softer ground conditions than those with green colors. The corresponding shaking building loss distribution is shown in Figure 6c. The loss values depend on shaking intensities, seismic vulnerability functions for the three building system elements, and total asset values. It can be observed that the ground shaking loss is widely distributed across the District of Tofino.

For the tsunami hazard and risk assessments, the high-resolution tsunami inundation simulation is carried out and the inundation depth distribution is obtained (Figure 6d). The inundation depth map clearly shows higher tsunami hazards in the beach areas that face the Pacific Ocean directly and are at low elevation (Figure 2b). Consequently, tsunami loss distribution in Tofino is concentrated in the beach areas (Figure 6e). When the shaking and tsunami losses are combined (Figure 6f), the expected total risk is widely spread across Tofino, with significant tsunami losses along the beaches.

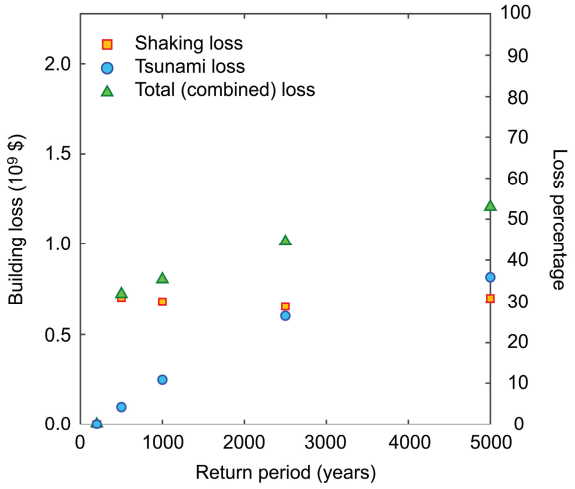

Figure 7: Shaking, tsunami, and total (combined) building loss for five earthquake rupture scenarios corresponding to the return periods of 200, 500, 1000, 2500, and 5000 years.

To summarize the multi-hazard loss results for Tofino, Figure 7 shows how the relative contributions of the shaking and tsunami losses to the total loss varies in terms of return period level. At low return period levels, shaking losses are dominant, whereas with the increase of return period level, tsunami losses become significant. The consideration of multi-hazard loss is important for Tofino because different local areas are affected by ground shaking and tsunami inundation significantly.

4. CONCLUSIONS

This study developed a new multi-hazard shaking-tsunami risk model for Tofino due to the Cascadia subduction earthquakes. The case study results for Tofino, BC, indicated that both shaking and tsunami risks must be considered because different local areas are affected by different hazards. In the future, more comprehensive multi-hazard risk assessments should be carried out by conducting detailed shaking and tsunami inundation loss estimations for all earthquake rupture scenarios. In addition, the damage accumulation due to shaking and tsunami should be considered. The framework is generic; therefore, once region-specific model components are developed, it can be applied to other coastal communities in active subduction regions.

5. FUNDING

The work was supported by the Canada Research Chair program (950-232015) and the NSERC Discovery Grant (RGPIN-2019-05898).

6. REFERENCES

Atkinson, G.M., and Adams, J. (2013). "Ground motion prediction equations for application to the 2015 Canadian national seismic hazard maps?" *Canadian Journal of Civil Engineering*, 40, 988–998.

De Risi, R., Goda, K., Yasuda, T., and Mori, N. (2017). "Is flow velocity important in tsunami empirical fragility modeling?" *Earth-Science Reviews*, 166, 64–82.

Goda, K., and Atkinson, G.M. (2010). "Intraevent spatial correlation of ground-motion parameters using SK-net data" *Bulletin of the Seismological Society of America*, 100, 3055–3067.

Goda, K., Yasuda, T., Mori, N., and Maruyama, T. (2016). "New scaling relationships of earthquake source parameters for stochastic tsunami simulation" *Coastal Engineering Journal*, 58, 1650010.

Goda, K., and De Risi, R. (2018). "Multi-hazard loss estimation for shaking and tsunami using stochastic rupture sources" *International Journal of Disaster Risk Reduction*, 28, 539–554.

Goda, K. (2019). "Time-dependent probabilistic tsunami hazard analysis using stochastic rupture sources" *Stochastic Environmental Research and Risk Assessment*, 33, 341–358.

Goda, K. (2022). "Stochastic source modeling and tsunami simulations of Cascadia subduction earthquakes for Canadian Pacific coast" *Coastal Engineering Journal*, 64, 575–596.

Goldfinger, C., et al. (2012). "Turbidite event history: methods and implications for Holocene paleoseismicity of the Cascadia subduction zone" *United States Geological Survey Professional Paper 1661–F*.

Goto, C., Ogawa, Y. Shuto, N., and Imamura, F. (1997). "Numerical method of tsunami simulation with the leap-frog scheme" IOC Manual, UNESCO, No. 35, Paris, France.

Hayes, G.P., et al. (2018). "Slab2, a comprehensive subduction zone geometry model" *Science*, 362, 6410, 58–61.

Leonard, L.J., Rogers, G.C., and Mazzotti S. (2014). "Tsunami hazard assessment of Canada" *Natural Hazards*, 70, 237–274.

Mai, P. M., and Beroza, G. C. (2002). "A spatial random field model to characterize complexity in earthquake slip" *Journal of Geophysical Research: Solid Earth*, 107, 2308.

Satake, K., Wang, K., and Atwater, B. F. (2003). "Fault slip and seismic moment of the 1700 Cascadia earthquake inferred from Japanese tsunami descriptions" *Journal of Geophysical Research: Solid Earth*, 108: B11, 2535.

Walton, M., et al. (2021). "Toward an integrative geological and geophysical view of Cascadia subduction zone earthquakes" *Annul Review of Earth and Planetary Sciences*, 49, 367–398.